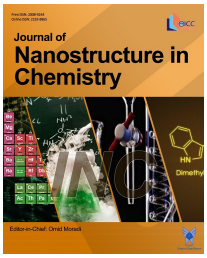

Volume 15, Issue 5, 152519 (1-21)

Journal of Nanostructure in Chemistry (JNSC)

https://doi.org/10.57647/jnsc.2025.1505.19

A New Heterogeneous PMO@MXene Catalyst for One-Pot Synthesis of Substituted 5-amino-3-(aryl)-1-phenyl-1*H*-pyrazole-4-carbonitrile Derivatives

Safa Hanifi[1], Farhad Shirini[1,*], Bahram Ramezanzadeh[2], Hassan Tajik[1]

[1]*Department of Organic Chemistry, Faculty of Chemistry, University of Guilan, Rasht, Iran.*
[2]*Department of Surface Coating and Corrosion, Institute for Color Science and Technology, Tehran, Iran.*

[*]**Corresponding author:** shirini@guilan.ac.ir

Original Research

Received:
2 July 2025
Revised:
12 August 2025
Accepted:
4 October 2025
Published online:
17 October 2025

Abstract:

In this study, we report the development of a novel and efficient MXene-based heterogeneous catalyst, PMO@MXene, for the green synthesis of 5-amino-3-(aryl)-1-phenyl-1*H*-pyrazole-4-carbonitrile derivatives. By integrating periodic mesoporous organosilica (PMO) into multilayered MXene, a hybrid nanocomposite was achieved that benefits from the high surface area and electrical conductivity of MXene along with the well-defined mesoporosity of PMO. This unique synergy enabled highly efficient catalytic performance under mild, eco-friendly conditions, requiring only a small amount of catalyst and allowing for easy recovery and reuse with minimal loss of activity. The pyrazole derivatives, known for their potential pharmaceutical relevance, were obtained in excellent yields and characterized using standard spectroscopic techniques. Importantly, this work highlights the potential of the PMO@MXene as a sustainable and recyclable heterogeneous catalyst platform for the synthesis of biologically significant heterocyclic compounds.

Keywords: MXene; Periodic mesoporous organosillica; Pyrazole; Ti_3AlC_2; PMO; Heterogeneous catalyst; Nanocomposite

Cite this article: Hnaifi, S., Shirini, F., Ramezanzadeh, B., Tajik, H. A New Heterogeneous PMO@MXene Catalyst for One-Pot Synthesis of Substituted 5-amino-3-(aryl)-1-phenyl-1*H*-pyrazole-4-carbonitrile Derivatives. *J Nanostruct Chem* **15**(5), 152519 (2025).

1. Introduction

Catalysis plays an essential role in modern chemical industries and environmental applications, particularly in the development of green and sustainable processes. In recent years, increasing attention has been directed toward designing heterogeneous catalysts with high activity and recyclability to address both synthetic efficiency and environmental concerns [1–3]. Supported catalysts in heterogeneous catalysis commonly employ materials such as ordered mesoporous silica (e.g., SBA-15, MCM-41) due to their high surface area and well-defined pore structures, facilitating efficient dispersion of active species [4]. The combination of PMO with MXene, a two-dimensional transition metal carbide/nitride with excellent electrical conductivity and surface area, produces a hybrid support with synergistic properties. In this study, PMO@MXene was selected to leverage these advantages, offering efficient catalysis under mild and green conditions, excellent recyclability, and enhanced durability compared to conventional supports [5–8]. Periodic mesoporous organosilicas (PMOs) further improve catalyst stability and functional group incorporation through organic-inorganic hybrid frameworks [9–11]. Porous materials are among the most effective supports for producing heterogeneous catalysts. A notable member of this family is PMO materials, a novel class of ordered mesoporous organosilicas that was first introduced in 1999 [12, 13]. These compounds can be synthesized through the

hydrolysis and condensation of organo-bridged alkoxysilanes ($(R'O)_3Si\text{-}R\text{-}Si(OR')_3$), where R′ is methyl or ethyl and R is an organic functional group, around a soft template [14, 15]. In this class of materials, the organosilica bridge embedded within the pore walls offers several advantages over pure ordered silica materials such as MCM-41 or SBA-15. These benefits include enhanced mechanical and hydrothermal stability, reduced pore blocking, increased hydrophobicity, and improved stability in water [16, 17]. Moreover, the uniform pore size, large pore volume, high surface area, and remarkable thermal and mechanical stability of PMOs make them highly desirable for a wide range of applications. These distinctive properties cause PMOs to be excellent candidates for essential fields such as ion exchange, separation, drug delivery, battery technology, fuel cells, sensors, catalysts, and chromatography [18].

MXenes are a diverse family of layered 2D nanomaterials derived from transition metal carbides, nitrides, or carbonitrides. They exhibit a variety of aspect ratios and consist of only a few atomic layers in thickness [19–21]. MXenes exhibit high electrical conductivity, exceptional solvent compatibility and stability, strong hydrophilicity, remarkable electrochemical properties, impressive mechanical strength, and surface area, 2D surface reactivity [22]. MXenes possess a versatile chemistry due to the selection of M and X elements, as well as surface terminating groups. These groups are crucial as a reactive layer on the MXene surface, facilitating the attachment of drugs and enzymes and enhancing their activity [23]. The general formula for MXenes is $M_{n+1}X_nT_x$, where M represents an early transition metal, such as Ti, X denotes carbon and/or nitrogen, and T corresponds to surface functional groups, including OH, F, or O. The variable x indicates the number of functional groups, while n is an integer ranging from 1 to 4 [24]. Many of the MXenes discovered have been synthesized through the selective etching of MAX phase materials [25, 26], where A can be elements such as Al, Si, P, S, Ga, etc. [27]. However, selective etching has only been successfully demonstrated for the removal of Al or Si from the MAX structure to produce MXenes [28, 29]. Until now, MXenes have been widely used as photoelectrocatalysts and electrochemical catalysts, but they have not been utilized as co-catalysts in multicomponent reactions. A distinguishing feature of our work is our novel use of MXene as a co-catalyst for the first time in these types of reactions. Multi-component reactions (MCRs) offer significant advantages over conventional multi-step reactions. They involve the one-pot condensation of three or more reactants, often in aqueous media, leading to high product yields with minimal or no by-products [30]. Pyrazole is a crucial heterocyclic scaffold in medicinal chemistry and organic synthesis [31]. While naturally occurring pyrazole-containing compounds are relatively rare, recent trends highlight the growing significance of the pyrazole ring in drug development pipelines [32, 33]. Pyrazole is a five-membered aromatic heterocycle containing two adjacent nitrogen atoms [34, 35]. The N-1 atom exhibits properties similar to the NH group in pyrrole, functioning as a hydrogen bond donor, while the N-2 atom resembles the nitrogen in pyridine, acting as a hydrogen bond acceptor (Figs. 1, 2) [33]. Several protocols have been developed for the synthesis of pyrazole derivatives, utilizing traditional thermal methods [36, 37], microwave or ultrasonic irradiation [38], or room-temperature reactions [39], often involving volatile organic solvents. Also, a wide range of both heterogeneous and homogeneous catalysts have been explored in pyrazole synthesis, including metal catalysts, metal complexes with various ligands, organocatalysts, and other catalytic systems [40, 41]. Among the diverse derivatives of these compounds, the synthesis of 5-amino-3-(aryl)-1*H*-pyrazole-4-carbonitrile derivatives faces several challenges, including the use of toxic solvents, expensive catalysts, and complex work-up procedures. The distinctive properties of these derivatives, coupled with the existing difficulties in their synthesis, have motivated us to explore innovative and efficient methods. Building on our commitment to synthesizing organic heterocycles through the principles of green chemistry and utilizing nanocatalysts [42–44], we have developed a novel approach that leverages the catalytic potential of the heterogeneous PMO@MXene nanocomposite. This method aims to overcome current challenges and enhance the overall efficiency of the mentioned synthetic process.

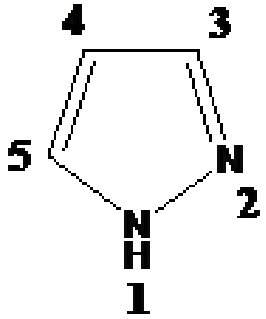

Figure 1. The structure of pyrazole.

2. Experimental

2.1 Materials and characterization techniques

All substrates used in this study, including ethanol, tetraethyl orthosilicate (TEOS, Merck), Pluronic P123 (average Mn $\sim$ 14,600, Merck), bis[3-(trimethoxysilyl) propyl] amine (BTPA, Merck), hydrochloric acid (HCl 37%, Merck), lithium fluoride (LiF- 99.99 Suprapur, Merck), Maxphase (Ti_3CAl_2-purity of $\geq$ 98%, 200 meshes purchased from Ningbo Beijiaer New Material Co., Ltd.), 3-aminopropyl triethoxysilane (99% Merck), and various aldehydes, were purchased from were purchased from commercial sources. Pure distilled water and 96% ethanol were used as solvents. Thin-layer chromatography (TLC) experiments were conducted using a UV lamp emitting at a wavelength of 254 nm. Product identification was performed using a Shimadzu FTIR 8400S spectrometer with potassium bromide (KBr) disks. Additionally, ^{1}HNMR spectra were recorded on a Bruker Avance 500 spectrometer in DMSO-d_6 at ambient temperature. Melting points were determined using a 9100 Electrothermal apparatus, and values are reported without corrections. The yields

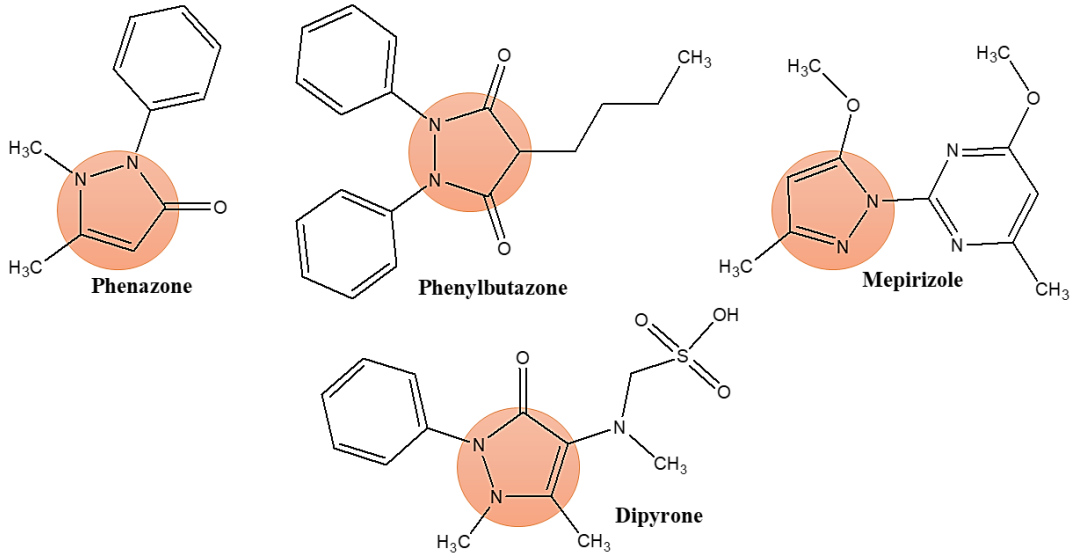

Figure 2. Commercial drugs containing pyrazole ring.

provided are based on the purified products obtained after the purification process.

2.2 MXene (Ti_3C_2) fabrication process

First, LiF (0.30 g) was stirred in HCl (37%, 7.50 mL) for 30 minutes. Then, the MAXphase (Ti_3AlC_2) (0.25 g) was gradually added to the mixture. The resulting solution was placed in a water bath at 34 °C for 72 hours. The product was collected by centrifugation, washed multiple times with HCl, ethanol, and water, and then dried in a vacuum oven (4 h, 0.19 g) (Fig. 3) [45].

2.3 Synthesis of amino-functionalized MXene

To start, 2.50 g of BTPA was added to a mixture of 1.0 g of deionized water (DW) and 9.0 g of EtOH, and the solution was stirred vigorously for 20 minutes. Following this, 0.10 g of pre-weighed MXene powder was immersed in the prepared solution. The mixture was then transferred to a single-neck round-bottom flask and refluxed at 80 °C for 24 hours with continuous stirring. After the reaction was completed, the resulting product was centrifuged using ethanol and deionized water to remove any leftover modifier. Finally, the product was dried in an oven at 75 °C for 24 hours to yield the amino-functionalized MXene (0.185 g).

2.4 Development of periodic mesoporous organosilica (PMO)

A mixture of 0.50 g of P123, 3.50 mL of ethanol, and 1.10 g of deionized water (DW) was mixed and stirred at 20 °C. Afterward, 1.69 mL of TEOS was added to the mixture and stirred continuously for 1 hour at 20 °C. Then, 0.70 mL of BTPA was introduced into the mixture in a dropwise manner, and the mixture was stirred for an additional hour. Lastly, the product was washed three times with water and dried at 60 °C for 24 hours.

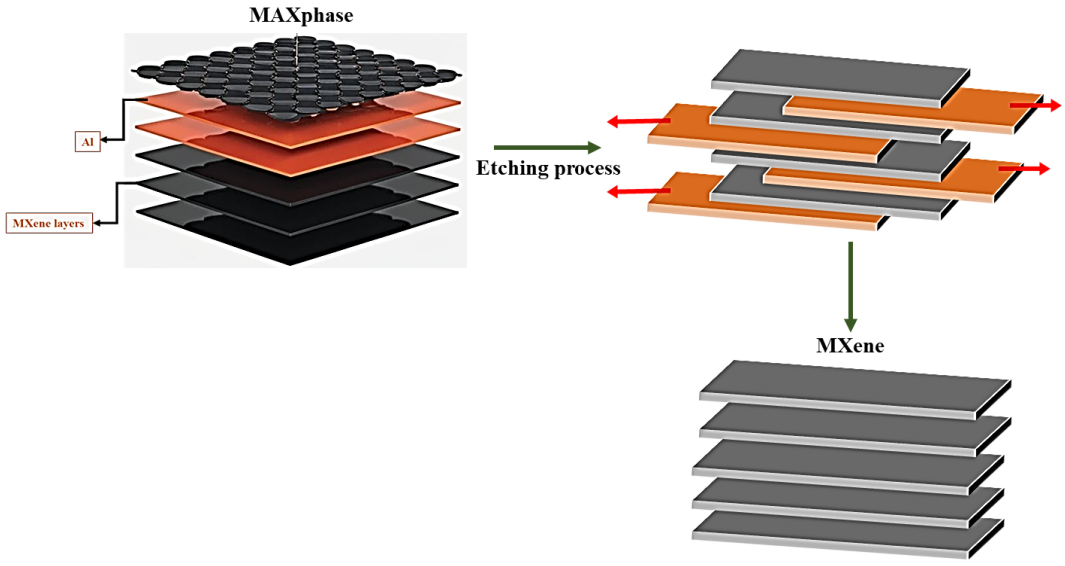

Figure 3. Schematic of the fabrication process of MXene.

2.5 Surfactant removal of PMO

To remove the surfactant, 0.250 g of the as-synthesized PMO was stirred in 37.5 mL of EtOH, followed by the addition of 0.850 mL of 36% HCl. This mixture was heated to 60 °C and maintained at that temperature for 24 h. After that, the solid product was collected by filtration, washed with EtOH, and subsequently dried in an oven at 60 °C for 24 h. The surfactant-free PMO was obtained after this process.

2.6 Fabrication of the PMO@MXene nanocomposite

The preparation of the PMO@MXene nanocomposite employs a physical synthesis method. In this procedure, 0.010 g of amino-functionalized MXene and 0.0030 g of PMO were mixed in 1.10 g of DW and 3.50 mL of EtOH. This mixture was stirred for 24 hours at 60 °C. Afterward, the separated solid residue was washed multiple times with water and ethanol, followed by drying at 75 °C for 24 hours (0.013 g) (Fig. 4).

2.7 General procedure for the synthesis of 5-amino-3-(aryl)-1-phenyl-1*H*-pyrazole-4-carbonitriles in the presence of the PMO@MXene nanocomposite

In a 5.0 mL reaction flask, a mixture of aldehyde (1a-l, 1.0 mmol), phenyl hydrazine (2, 1.0 mmol), malononitrile (3, 1.0 mmol), and the catalyst (5.0 mg) were combined in H_2O (2.0 mL) and heated under reflux for the required duration. The reaction progress was monitored using thin-layer chromatography (TLC, n-hexane: ethyl acetate (1:3)). Upon completion, the resulting solid, consisting of the desired product and the catalyst, was collected by filtration. The separation of the PMO@MXene nanocomposite from the target pyrazole derivatives was achieved by taking advantage of the solubility of pyrazole in ethyl acetate (EtOAc). Finally, highly pure pyrazole derivatives were obtained through crystallization from EtOAc.

3. Results and discussion

Various techniques were used to analyze their size, shape, composition, surface properties, and other key attributes. To confirm the structure and surface features of the synthesized PMO, MXene, and PMO@MXene nanoparticles, multiple analytical methods were utilized. Fourier transform infrared spectroscopy (FT-IR) was used to identify functional groups through vibrational modes, while field-emission scanning electron microscopy (FESEM) provided detailed imaging to examine size and morphology. Energy-dispersive X-ray spectroscopy (EDS) was used to determine the elemental composition, and X-ray powder diffraction (XRD) assessed the crystallinity and structural arrangement. High-resolution transmission electron microscopy (HRTEM) was used to imaging the mode of specialized transmission electron microscopes that allows for direct imaging of the atomic structure of samples.

3.1 FT-IR of PMO, MXene, and the PMO@MXene nanocomposite

The FT-IR spectrum of the synthesized PMO nanoparticles exhibits distinct characteristic peaks across the spectral range of $400 - 4000$ cm^{-1}. In this spectrum, the peak at 1470 cm^{-1} corresponds to the bending vibrations of the Si–O–Si bonds, while the peak at 1794 cm^{-1} is associated with the asymmetric stretching vibrations of Si–O–Si. The absorption at 940 cm^{-1} is attributed to the Si–OH stretching vibrations or Si–O–Si symmetric stretching vibrations. The peak at 1360 cm^{-1} is linked to the CH_3 vibrations or Si–CH_3 stretching vibrations, whereas the peak at 1472 cm^{-1} corresponds to the CH_2 bending vibrations. Additionally, the peaks at 2820 cm^{-1} and 2943 cm^{-1} are related to the symmetric stretching vibrations of CH_2, and CH_3, respectively. The broad peak at 3431 cm^{-1} is attributed to the O–H or N–H stretching vibrations.

The FT-IR spectrum of MXene provides crucial insights into its functional groups. In this spectrum, a broad absorption band around 3400 cm^{-1} corresponds to the stretching vibrations of the hydroxyl groups on the MXene surface, suggesting partial oxidation or surface modification. The peak near 1600 cm^{-1} is associated with the stretching vibrations of the metal–carbon (M–C) bonds, confirming the presence of a transition metal (such as Al) and carbon in the MXene structure. Furthermore, the peak around 1100 cm^{-1} corresponds to the Ti–O bending vibrations, indicat-

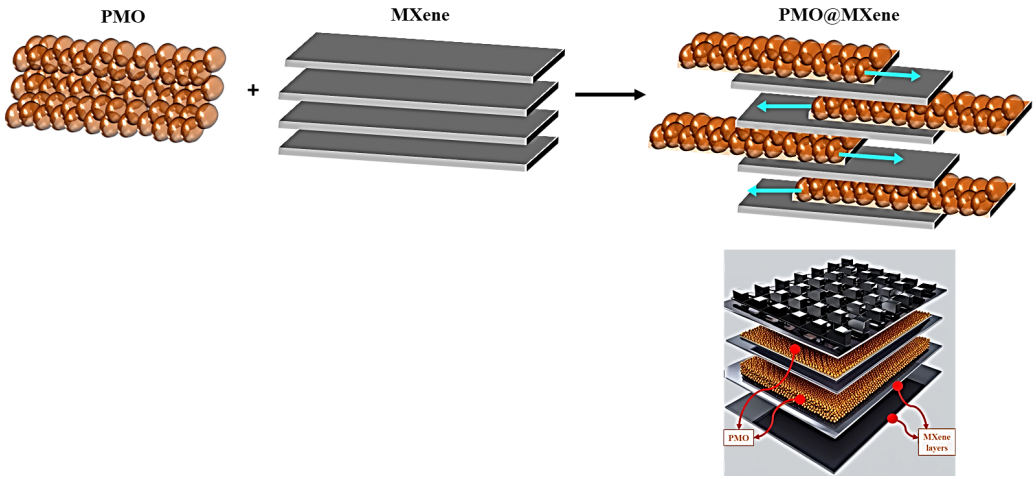

Figure 4. Schematic of the PMO@MXene nanocomposite.

ing partial oxidation of the MXene surface and the presence of metal–oxygen (M–O) functional groups.

The FT-IR spectrum of the PMO@MXene nanocomposite reveals several significant absorption bands, shedding light on its chemical structure and functional groups. For this reagent, a strong absorption band in the range of $1000-1200\ cm^{-1}$ corresponds to the symmetric and asymmetric stretching vibrations of the Si–O–Si bonds, characteristic of silica frameworks in PMOs, confirming their incorporation into the composite. The peaks in the $500-800\ cm^{-1}$ range indicate the bending vibrations related to the MXene functional groups, including M–O, M–C, or Ti–O bonds, depending on the MXene composition. The broad absorption band between $3000-3500\ cm^{-1}$ is attributed to the O–H stretching vibrations, originating from the hydroxyl groups on the surface or adsorbed water molecules, underscoring the composite's hydrophilic nature. Additionally, the peak at $1600\ cm^{-1}$ corresponds to the C=C stretching vibrations, indicating the presence of organic moieties, or it results from the H–O–H bending vibrations of the adsorbed water molecules (Fig. 5).

3.2 FESEM of PMO, MXene, and the PMO@MXene nanocomposite

Figures 6 (a) and 6 (a) present the SEM images of MXene, showcasing its distinctive accordion-like structure. The SEM images of the gels prepared with P123 are illustrated in Figs. 6 (c) and 6 (d). The SEM micrograph of the PMO gel reveals a mesoporous, cabbage-like structure. As depicted in the Figs. 6 (e) and 6 (f), the layers of MXene are separated, with the metal component removed through washing. PMO particles, which have created a physical composite with the MXene, are positioned both between and on the layers of MXene. Nanoartography, a method to make SEM images resembling the real world, is used for Scheme S2 and Fig. 6 (c).

3.3 Mapping elemental analysis of the PMO@MXene nanocomposite and EDS of PMO, MXene, and the PMO@MXene nanocomposite

The elemental mapping analysis of the PMO@MXene catalyst (Fig. 3) confirms the presence and homogeneous distribution of carbon (C), oxygen (O), silicon (Si), aluminum (Al), and titanium (Ti) throughout the nanocomposite. The uniformity of the elemental dispersion suggests the successful incorporation of PMO onto the MXene sheets. In particular, the signals from silicon and oxygen indicate the presence of the mesoporous silica framework, while those from titanium and aluminum originate from the MXene layers. Additionally, the energy-dispersive X-ray spectroscopy (EDS) analysis (Fig. 4) further supports these findings by clearly identifying the expected elements in each component: C, O, and Si for PMO; C, Ti, and Al for pristine MXene; and a combination of C, Ti, O, and Si for the PMO@MXene hybrid. These results collectively confirm the successful synthesis and integration of both components into a unified nanostructured material.

3.4 XRD of the PMO, MXene, and the PMO@MXene nanocomposite

The X-ray diffraction (XRD) patterns demonstrate the effects of the processes, such as etching and exfoliation, on the crystalline structure of PMO. XRD analysis of PMO reveals a single broad peak in the low-angle diffraction range ($1^\circ - 5^\circ$) at approximately $2\theta = 1.11^\circ$, corresponding to a well-ordered mesoporous structure. This confirms the presence of long-range mesostructural order due to the periodic arrangement of silica walls. Additionally, a broad peak in the $15 - 30^\circ$ range is characteristic of amorphous silica (SiO_2). Since PMO materials are predominantly amorphous, consisting of silica frameworks with organic bridges, distinct crystalline reflections are absent.

The combination of sharp MXene peaks with broad sec-

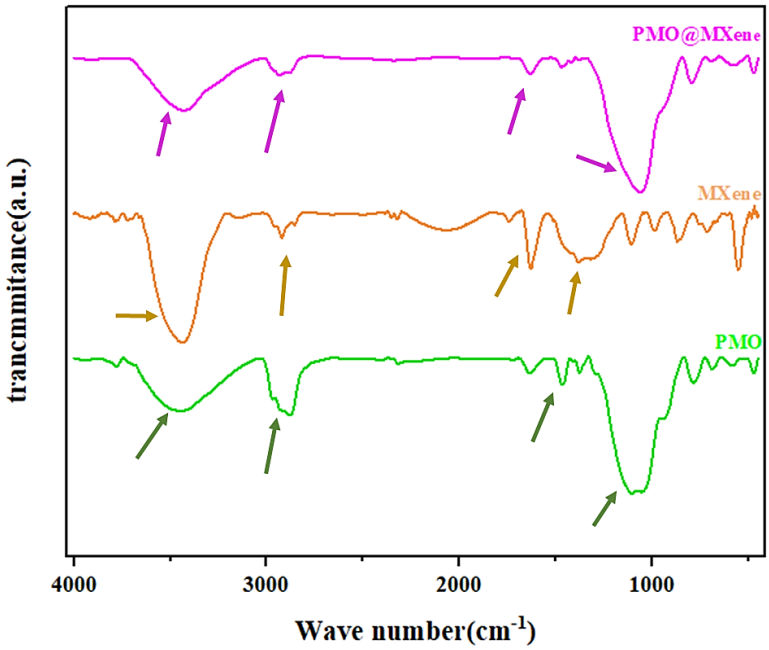

Figure 5. FT-IR of PMO, MXene, and the PMO@MXene nanocomposite.

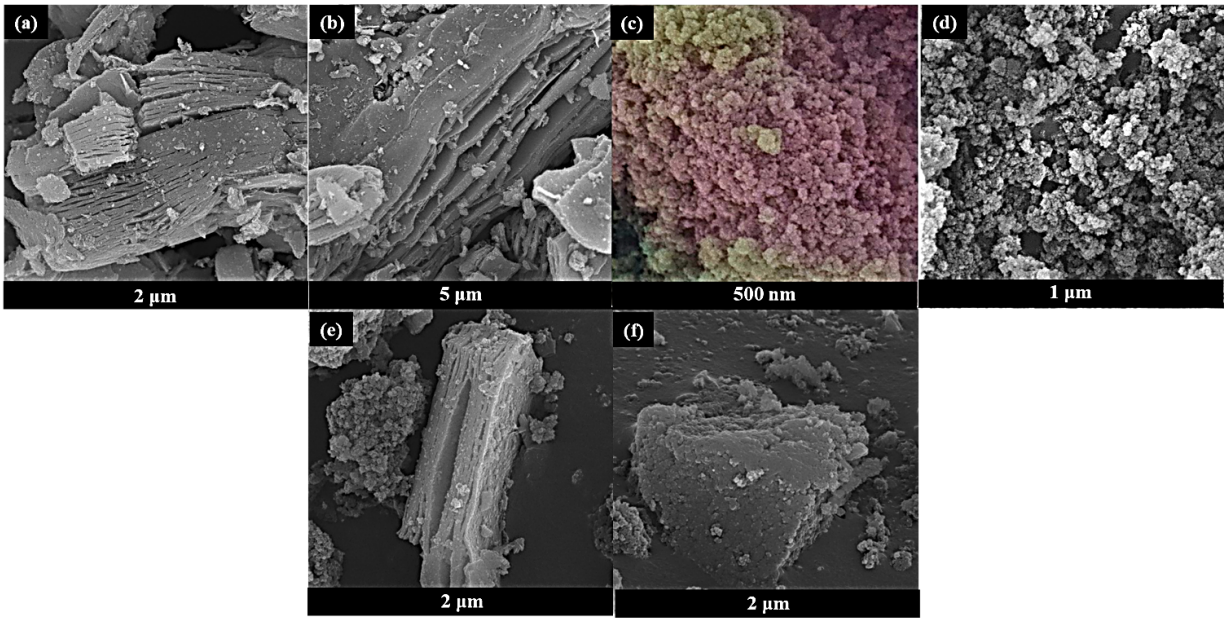

Figure 6. FESEM images of (a, b) MXene; (c, d) PMO, and (e, f) the PMO@MXene nanomposite.

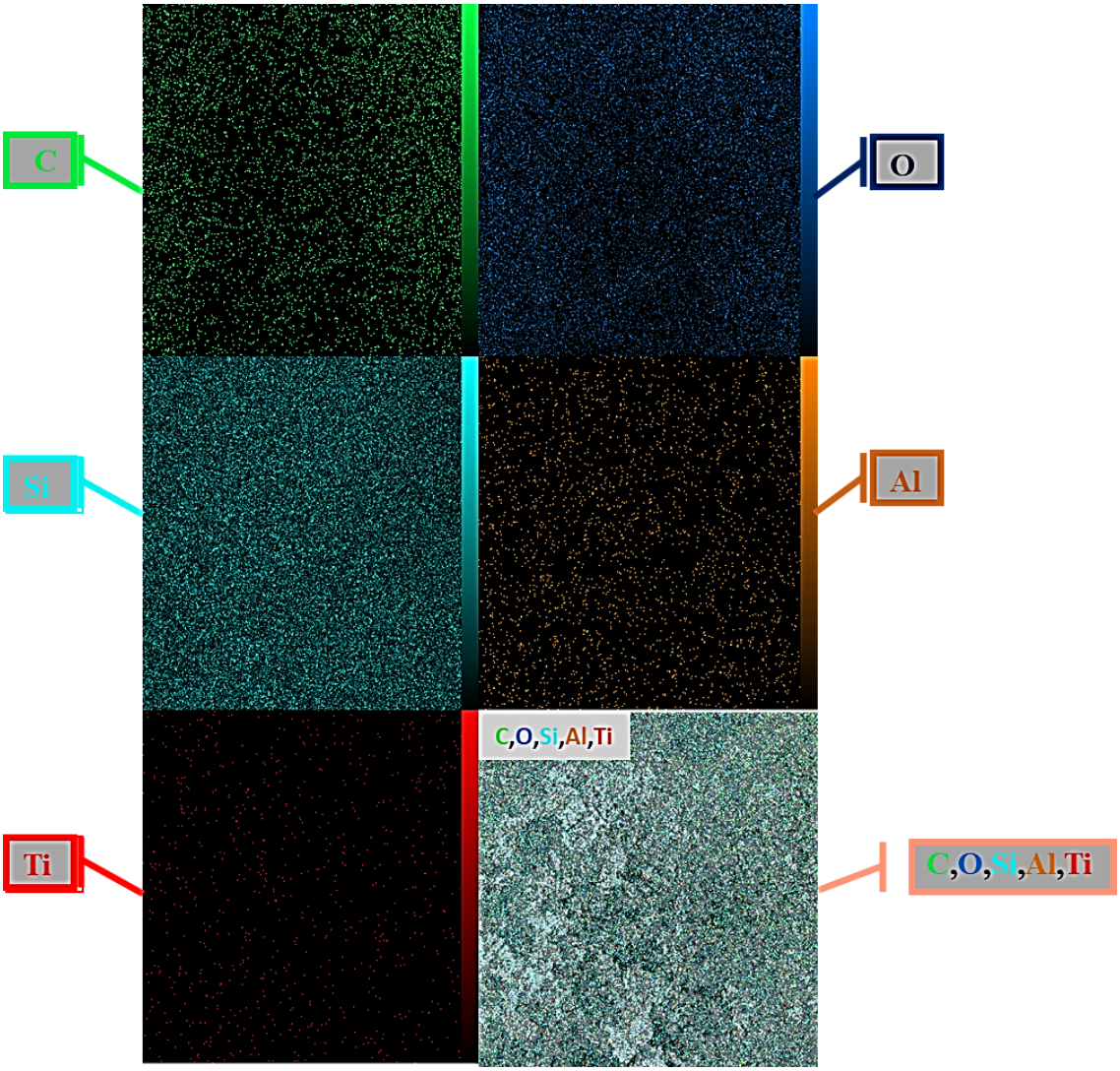

Figure 7. EDS elemental mapping analysis of the PMO@MXene nanocomposite.

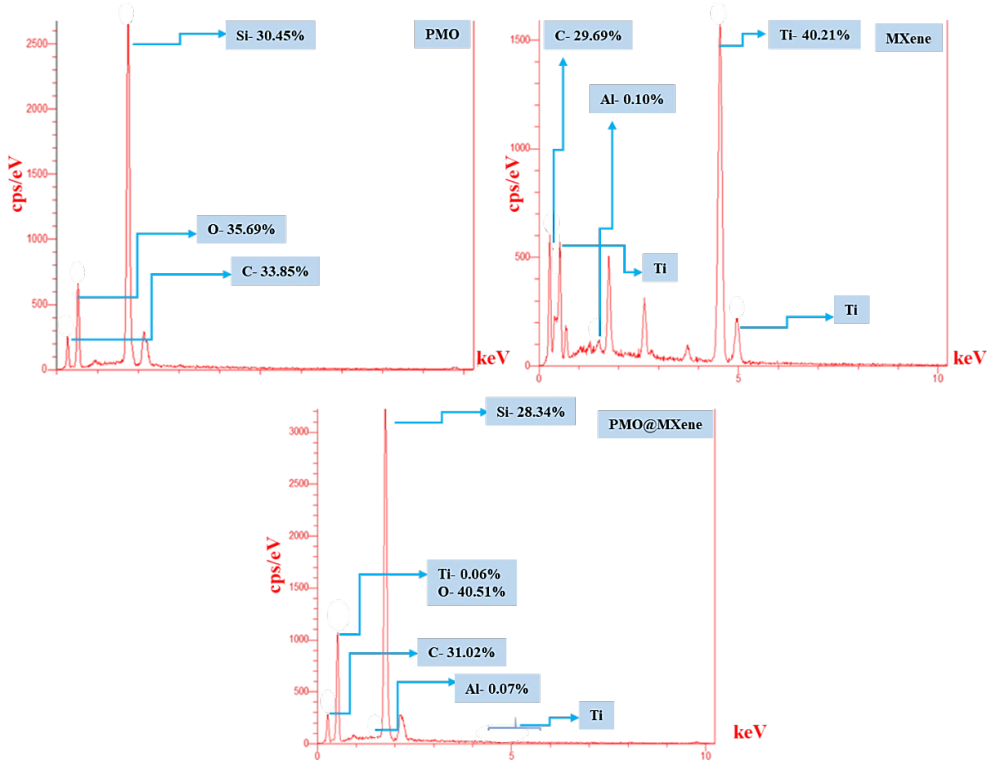

Figure 8. EDS of PMO, MXene, and the PMO@MXene nanocomposite.

ondary phase peaks provides clear evidence of the successful integration of PMO and MXene within the prepared composite. A sharp peak at $2\theta = 6.5°$ corresponds to the (002) reflection of the MAX phase, indicating an interlayer spacing of approximately 13.6 Å between the MXene layers. The high intensity of this peak suggests a significant proportion of well-ordered crystalline MXene within the composite. Broad peaks in the $2\theta = 20 - 30°$ range are associated with the secondary phases, such as TiC and Al_2O_3. The positions of these peaks align with the (111), (200), and (220) reflections of the TiC phase, as well as the (012), (104), and (110) reflections of the Al_2O_3 phase. Furthermore, the broad nature of these peaks suggests that the secondary phases are likely nanocrystalline or disordered. Additionally, broad peaks in the $2\theta = 40 - 60°$ range confirm the presence of nanostructured components, indicating the integration of the mesoporous silica framework within the MXene structure (Fig. 9).

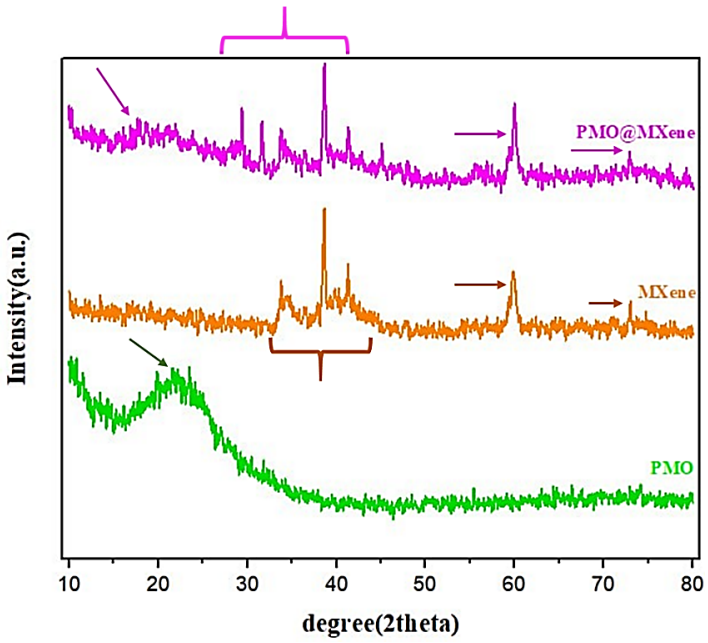

Figure 9. X-ray diffraction patterns of PMO, MXene, and the PMO@MXene nanocomposite.

Also employing Scherer's equation for particle size calculation at $2\theta = 38.66°$ and a full width at half maximum (FWHM) of 0.313 shows a determined particle size of 5.1 nm.

3.5 HRTEM, SEAD, and TEM of the PMO@MXene heterogeneous nanocomposite

As illustrated in Fig. 10, the obtained Miller index (1 0 0) located around the central spot and positioned lower in the labeling order, along with (1 0 1) and (4 0 2) for PMO (reference code: 00-033-1161), and the Miller indices (1 0 0), (1 0 4), (1 0 8), and (1 1 6) for MXene (reference code: 96-722-1325) from the SAED analysis, together with the d-spacing values of 3.41 Å and 2.71 Å determined through HRTEM analysis for the Miller indices (1 0 1) of PMO and (1 0 0) of MXene, respectively, indicate the successful synthesis of PMO@MXene.

The TEM images (Figs. 10 (c) and 10 (d)) demonstrate the successful immobilization of porous PMO domains on the layered MXene substrate. The uniform distribution and distinct contrast between the PMO particles and the MXene sheets confirm the formation of a well-defined PMO@MXene heterostructure, which is expected to enhance the catalytic performance due to the synergistic effects of high surface area and conductivity.

3.6 Systematic exploration of optimal conditions for the synthesis of 5-amino-3-(aryl)-1-phenyl-1*H*-pyrazole-4-carbonitrile (pyrazole) derivatives

Once the target reagent was identified, it was employed in the synthesis of 5-amino-3-(aryl)-1-phenyl-1*H*-pyrazole-4-carbonitrile derivatives to evaluate its catalytic performance. Table 1 details the optimization of the synthesis of a 5-amino-3-(aryl)-1-phenyl-1*H*-pyrazole-4-carbonitrile derivative through a three-component reaction involving phenylhydrazine, 2-bromobenzaldehyde, and malononitrile, each at a concentration of 1.0 mmol. The study systematically explored various parameters, including temperature, solvent type, catalyst type, amount, and reaction time. The primary focus was on the use of PMO@MXene as a catalyst, assessing its effectiveness at both room temperature and elevated temperatures (80 °C) across different solvents, including

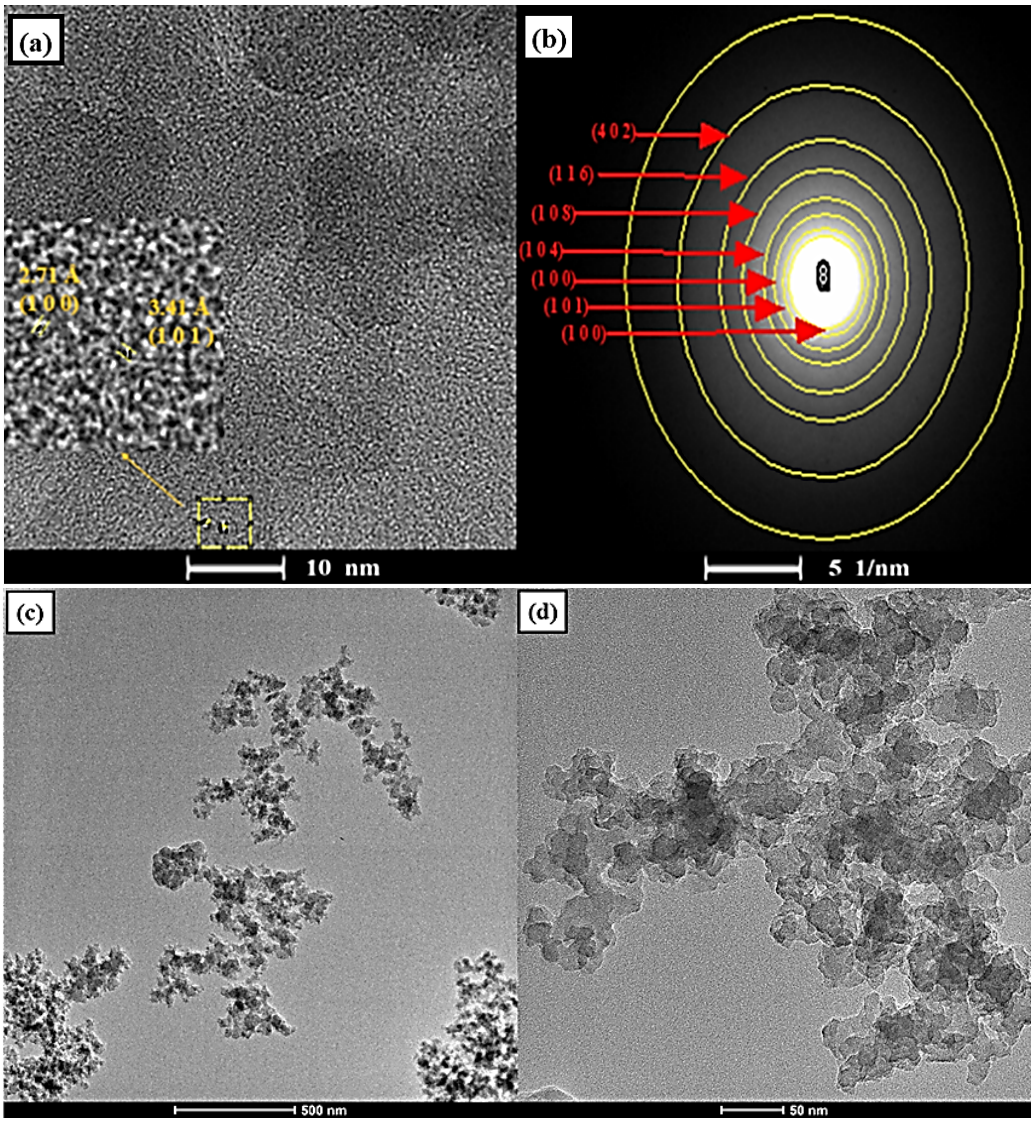

Figure 10. (a) HRTEM analysis, (b) SAED, and (c and d) TEM analysis of the PMO@MXene nanocomposite.

Table 1. Optimization study for the synthesis of 5-amino-3-(aryl)-1-phenyl-1*H*-pyrazole-4-carbonitrile under the effect of the PMO@MXene nanocomposite.[a].

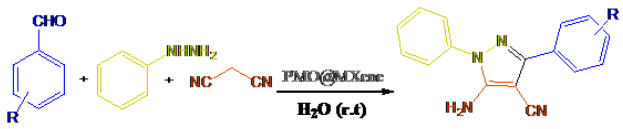

(1) (2) (3) (4)

Entry	Catalyst loading (mg)	Solvent (mL)	Temperature (°C)	Time (min.)	Yieldb(%)
1	-	-	r.t	65	-
2	-	H_2O (2.0)	r.t	60	21
3	PMO	H_2O (2.0)	r.t	55	36
4	MXene	H_2O (2.0)	r.t	50	41
5	PMO@MXene (2.0)	H_2O (2.0)	r.t	45	75
6	PMO@MXene (5.0)	H_2O (2.0)	r.t	15	94
7	PMO@MXene (5.0)	EtOH (2.0)	r.t	50	32
8	PMO@MXene (5.0)	EtOAc (2.0)	r.t	60	28
9	PMO@MXene (5.0)	CH_2Cl_2 (2.0)	r.t	40	30
10	PMO@MXene (5.0)	H_2O/EtOH (2.0)	r.t	45	41
11	PMO@MXene (5.0)	-	80	45	48
12	PMO@MXene (5.0)	-	80	30	68
13	PMO@MXene (7.50)	-	80	20	85
14	PMO@MXene (5.0)	-	80	20	31
15	-	-	80	25	-

[a] Reaction condition: aldehyde (1, 1.0 mmol), phenyl hydrazine (2, 1.0 mmol), malononitrile (3. 1.0 mmol), and 2.0 mL of H_2O as a solvent.
[b] The yield refers to the isolated pure product 4.

water, ethanol, ethyl acetate, and dichloromethane, and also under solvent-free conditions. The results were evaluated based on the product yield, which was determined after purification via recrystallization in ethyl acetate or chloroform. The optimal conditions for the synthesis of the requested product were achieved using 5.0 mg of the PMO@MXene nanocatalyst in water at room temperature, resulting in a remarkable 94% yield in just 15 minutes (Table 1, entry 6). Solvent-free conditions at 80 °C in the presence of 7.50 mg of the catalyst also yielded favorable results, achieving an 85% yield within 20 minutes (Table 1, entry 13). In contrast, reactions conducted without a catalyst or in alternative solvents such as ethanol (32%), ethyl acetate (28%), and dichloromethane (30%) showed significantly lower effectiveness, underscoring the critical role of the catalyst-solvent combination. Notably, when water was used as a solvent without a catalyst, a moderate yield of 21% was recorded (Table 1, entry 2), which improved to 75% with the addition of 2.0 mg of the catalyst (Table 1, entry 5), illustrating the catalyst's positive influence even in minimal amounts.

This optimization study emphasizes the efficiency of employing 5.0 mg of the PMO@MXene heterogeneous nanocomposite as a catalyst at room temperature, facilitating a rapid and high-yield (94%) synthesis of 5-aminopyrazole-4-carbonitriles under environmentally friendly conditions. The significant role of water as a green solvent, along with the potential of solvent-free conditions, aligns with sustainable chemistry principles. The systematic investigation of the reaction parameters offers a valuable framework for developing efficient synthetic strategies for 5-amino-3-(aryl)-1-phenyl-1*H*-pyrazole-4-carbonitrile derivatives, which hold significance in pharmaceutical and materials science.

Subsequently, various aromatic aldehydes were employed under the optimized conditions, resulting in the successful formation of the anticipated products with good to excellent yields and in highly favorable reaction times (Table 2).

3.7 Proposed mechanism for the synthesis of 5-amino-3-(aryl)-1-phenyl-1*H*-pyrazole-4-carbonitriles (4a-l) catalyzed by the PMO@MXene nanocomposite

This reaction is a multicomponent reaction (MCR) in which malononitrile, an aromatic amine (phenyl hydrazine), and an aldehyde combine to form a fused heterocyclic system. In the first step, the aldehyde is activated by the catalyst, and

Table 2. Synthesis of 5-amino-3-(aryl)-1-phenyl-1*H*-pyrazole-4-carbonitriles (4a-l) using various aldehydes in the presence of PMO@MXene.

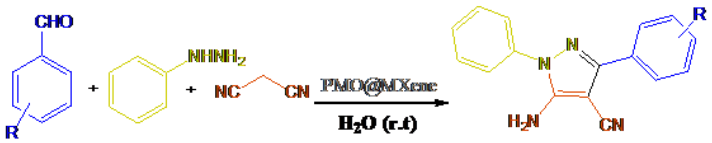

(1) (2) (3) (4)

Entry	Aldehyde (a-l)	Product (a-l)	Time (min.)	Yield[a] (%)	M.P. (°C)	M.P. (°C) [Ref.]
1	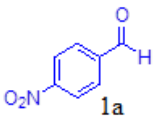 1a	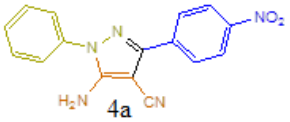 4a	15	87	154-156	154-156 [46]
2	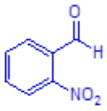 1b	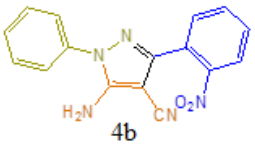 4b	20	85	162-165	159-161 [47]
3	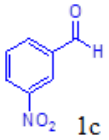 1c	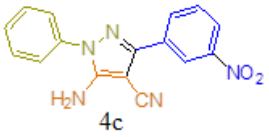 4c	20	90	126-128	127-129 [48]
4	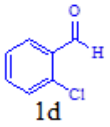 1d	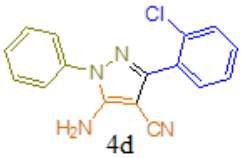 4d	15	94	Semi-solid	Semi solid [47]
5	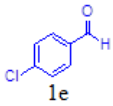 1e	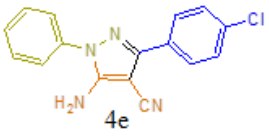 4e	15	91	126-128	126-128 [46]
6	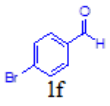 1f	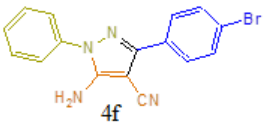 4f	25	86	163-166	164-165 [47]
7	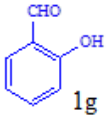 1g	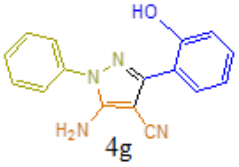 4g	25	89	159-162	161-162 [47]

Reaction conditions: Aromatic aldehyde (1a–l, 1.0 mmol), phenyl hydrazine (2, 1.0 mmol), malononiteile (3, 1.0 mmol), catalyst (5.0 mg), and DW (2.0 mL) under reflux conditions. [a]The yields refer to the isolated pure products.

Continued of Table 2.

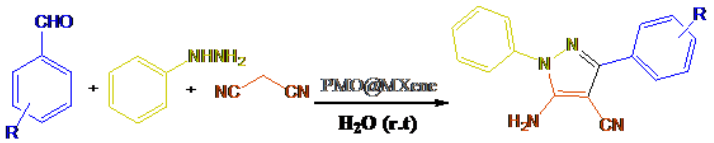

(1) (2) (3) (4)

Entry	Aldehyde (a-l)	Product (a-l)	Time (min.)	Yield[a] (%)	M.P. (°C)	M.P. (°C) [Ref.]
8	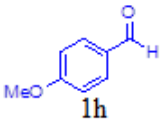	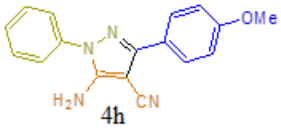	20	93	109-110	107-108 [47]
9	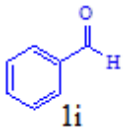	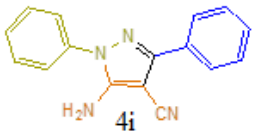	15	91	154-157	156-158 [48]
10	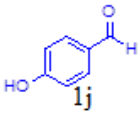	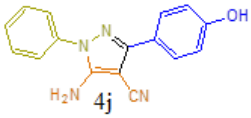	25	86	207-210	208-210 [47]
11	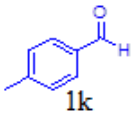	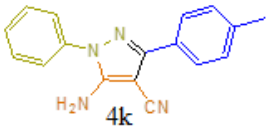	20	89	116-118	117-118 [47]
12	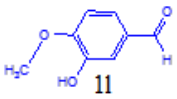	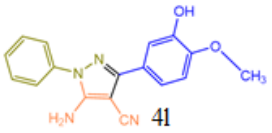	25	90	200-220	New sample

Reaction conditions: Aromatic aldehyde (1a–l, 1.0 mmol), phenyl hydrazine (2, 1.0 mmol), malononiteile (3, 1.0 mmol), catalyst (5.0 mg), and DW (2.0 mL) under reflux conditions. [a]The yields refer to the isolated pure products.

malononitrile, acting as a nucleophile, attacks it to generate a reactive intermediate. Next, malononitrile adds to this intermediate, leading to the formation of a new C–N bond. Subsequently, several proton transfers and rearrangements take place within the structure, giving rise to a more stabilized conjugated intermediate. In the following step, the nitrogen atom of the malononitrile attacks one of the activated carbons bonded to cyano groups, resulting in cyclization and the formation of a new ring. This ring closure ultimately produces a heterocyclic scaffold. In the final stage, further proton shifts restore aromaticity and enhance stability, yielding the final product as an indole or pyridine derivative substituted with cyano and aromatic groups. Thus, through a one-pot multicomponent reaction, the desired heterocyclic compound is efficiently synthesized (scheme 1).

3.8 Investigation of the recyclability and reusability of the PMO@MXene nanocatalyst

The recyclability of the PMO@MXene nanocomposite was evaluated to assess its potential for repeated use. For this purpose, the catalyst was separated from the reaction mixture using a filter paper and subsequently washed with ethyl acetate and ethanol to eliminate any impurities. After being dried at 70 °C for 2 hours, the catalyst was reused in the same model reaction. As shown in Fig. 11, the recycled PMO@MXene catalyst demonstrated high conversion rates across multiple runs of the model reaction, indicating its effective catalytic activity. After six iterations using the recycled catalyst, an average yield of 92.6% was achieved. These results underscore the stability and recyclability of the PMO@MXene nanocomposite as a suitable het-

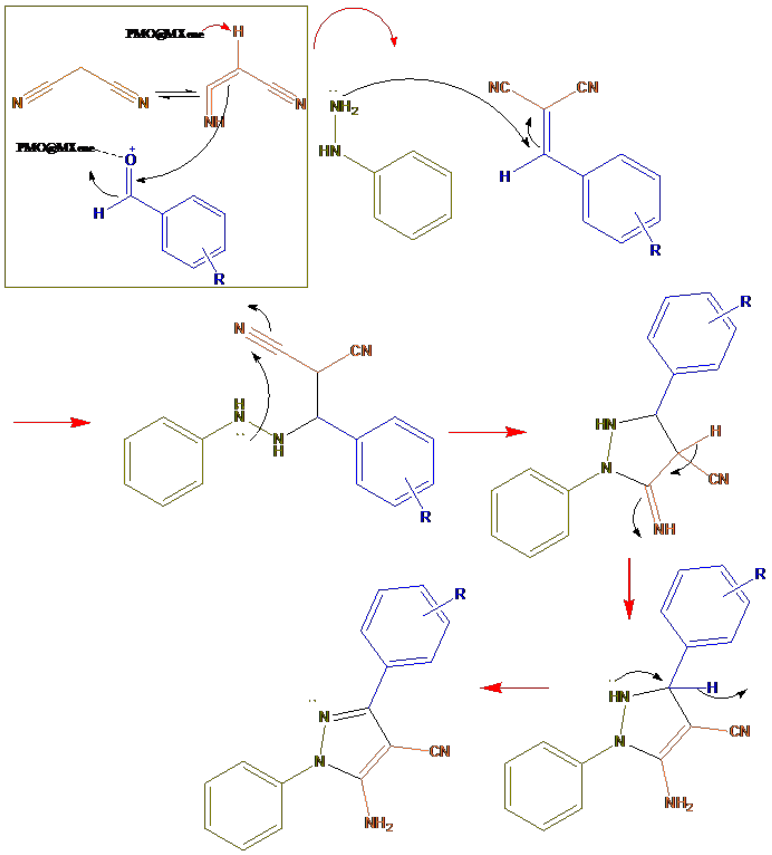

Scheme 1. The proposed mechanism for the synthesis of 5-amino-3-(aryl)-1-phenyl-1*H*-pyrazole-4-carbonitrile derivatives in the presence of the PMO@MXene catalyst.

erogeneous catalyst for the three-component reaction of 5-amino-3-(aryl)-1-phenyl-1*H*-pyrazole-4-carbonitrile (pyrazole) derivatives. The maintained high conversion efficiency of the recycled catalyst demonstrates its reusability without significant loss in activity. As shown in Fig. 12, the FT-IR spectra of the nanocomposite indicate that no significant change is observed in the structure of the PMO@MXene nanocatalyst after 6 runs. Overall, these findings highlight the promising potential of the PMO@MXene nanoparticles as a stable and efficient heterogeneous promoter under optimal reaction conditions.

3.9 Comparison of the efficiency of the recently reported protocols with our selected method in the synthesis of 5-amino-3-(aryl)-1-phenyl-1*H*-pyrazole-4-carbonitrile

As shown in Table 3, the performance of PMO@MXene was compared with several recently reported catalysts in terms of reaction time, yield, catalyst loading, and reaction conditions.

Notably, the PMO@MXene heterogeneous catalyst (entry 6) demonstrated a high yield (94%) comparable to the best-

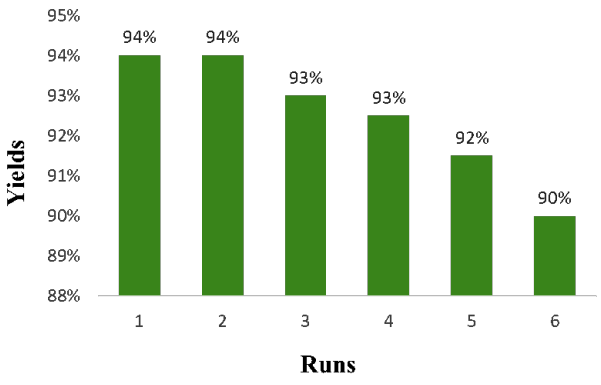

Figure 11. The recyclability and reusability of the PMO@MXene nanocomposite in the model reaction.

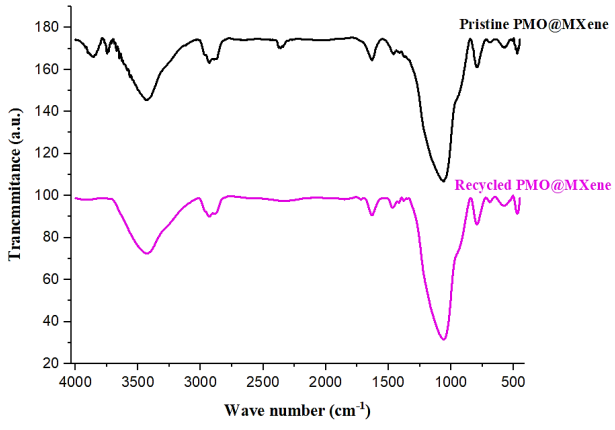

Figure 12. FT-IR spectrum of the pristine and recycled PMO@MXene nanocomposite after 6 runs.

Table 3. Comparison of the model reaction for the synthesis of 5-amino-3-(aryl)-1*H*-pyrazole-4-carbonitrile in the presence of PMO@MXene in terms of yield and time with some of the recent protocols.

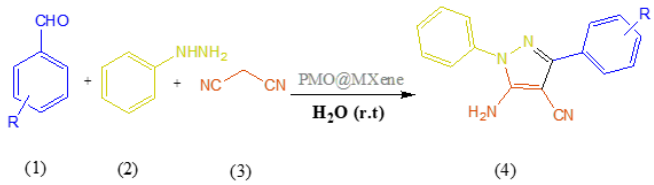

(1) (2) (3) (4)

Entry	Catalyst, loading	Reaction condition	Time (min.)	Yield (%)	Ref.
1	Fe_3O_4@SiO_2@Si(OEt)$(CH_2)_3$@melamine@TC, 0.050 g	65 °C/solvent free	7	78	[49]
2	Fe3O4@CQD@Si(OEt)$(CH_2)_3$NH@CC@Ad@Cu$(OAc)_2$, 0.050 g	65 °C/solvent-free	7	62	[50]
3	1,4-Diazabicyclo [2.2.2]octane (DABCO), 0.10 mmol	r.t/H_2O:EtOH (1;1)	10	97	[51]
4	$CoFe_2O4$@SiO_2@CPTES@Melamine, 10.0 mg	r.t/ H_2O	20	94	[52]
5	[4CSPy]$ZnCl_3$, 10.0 mol%	80 °C/solvent-free	30	95	[53]
6	PMO@MXene 5.0 mg (2.7 wt%)	r.t/H_2O	15	94	This work

performing methods (e.g., entries 3, 4, and 5), under milder and greener conditions, namely, at room temperature in water and using a significantly lower amount of catalyst (5.0 mg). In contrast, many other protocols require higher temperatures, solvent-free conditions, or higher catalyst loadings.

This comparison clearly illustrates the efficiency and sustainability advantages of the PMO@MXene as a green heterogeneous nanocatalyst.

4. Conclusion

In this research, for the first time, a new nanocomposite based on MXene formulated as PMO@MXene was prepared and identified. In continuation, the catalytic ability of this reagent was investigated in the synthesis of pharmacologically active 5-amino-3-(aryl)-1*H*-pyrazole-4-carbonitriles. The catalytic performance of PMO@MXene was found to be significantly influenced by solvent choice and temperature. The desired 5-amino-3-(aryl)-1*H*-pyrazole-4-carbonitrile derivatives were efficiently synthesized in water, a green solvent, via a one-pot, three-component reaction strategy. This method offers several key advantages, including high to excellent yields ($85-94\%$), low catalyst loading, and short reaction times. Furthermore, it eliminates the need for toxic organic solvents, simplifies product purification, facilitates an easy work-up process, and allows for the recyclability and reusability of the PMO@MXene heterogeneous catalyst. This environmentally friendly approach highlights the catalyst's potential for promoting more sustainable and efficient green chemistry practices.

Acknowledgement
We are thankful to the University of Guilan Research Council for the partial support of this work.

Authors Contribution
Safa Hanifi: Writing-original draft, methodology, investigation. Farhad Shirini: Validation, formal analysis, conceptualization, writing the final draft. Hassan Tajik and Bahram Ramezanzade: Conceptualization, formal analysis, investigation, writing- original draft.

Availability of data and materials
Data availability is detailed in the article and its Supplementary information section. Source data are also provided alongside the publication.

Conflict of interests
The authors declare that they have no known competing financial interests or personal relationships that could have appeared to influence the work reported in this paper.

References

[1] M. Melchionna and P. Fornasiero. "What Is to Be Expected from Heterogeneous Catalysis in the Pipeline to Circular Economy?". *Chem Sus Chem.*, **18**(5):e202402064, 2025.

[2] S. Wacławek. "Greener Catalysis for Environmental Applications: MDPI-Multidisciplinary ". Digital Publishing Institute, 2022.

[3] M. Haghighat, F. Shirini, and M. Golshekan. "Periodic mesoporous organosilica containing bridges with N-sulfonic acid groups: A new catalyst for the efficient formylation of amines and alcohols". *Silicon*, **12**(9):2087–98, 2020.

[4] Y. Zou, Z. Sun, Q. Wang, Y. Ju, N. Sun, Q. Yue, et al. "Core–Shell Magnetic Particles: Tailored Synthesis and Applications ". Chem Rev.(2):972–1048, 2024.

[5] A. Bordet, W. Leitner, and B. Chaudret. "Magnetically Induced Catalysis: Definition, Advances, and Potential". *Angewandte Chemie International*, **64**(24):e202424151, 2025.

[6] M. Mohammadi, M. Khodamorady, B. Tahmasbi, K. Bahrami, and A. Ghorbani-Choghamarani. "Boehmite nanoparticles as versatile support for organic–inorganic hybrid materials: Synthesis, functionalization, and applications in eco-friendly catalysis". *J Ind Eng Chem.*, **97**:1–78, 2021.

[7] A. Reina, R. Carmona-Chávez, I.T. Pulido-Díaz, D. Martínez, K.P. Salas-Martin, and I. Guerrero-Ríos. "Silica-Supported 1st Row Transition Metal (Nano) Catalysts: Synthetic and Catalytic Insight". *Chem Cat Chem.*, **15**(11):e202300285, 2023.

[8] X. Yu and C.T. Williams. "Recent advances in the applications of mesoporous silica in heterogeneous catalysis". *Cat Sci Technol.*, **12** (19):5765–94, 2022.

[9] A. Erigoni and U. Diaz. "Porous silica-based organic-inorganic hybrid catalysts: A review". *Catalysts*, **11**(1):79, 2021.

[10] A. Amirsoleimani, Z. Bahrami, and K. Kafshdouzan. "Synthesis of a novel antibacterial nanocomposite based on periodic mesoporous organosilica, zinc oxide, and medical leech saliva as a nanocarrier for streptomycin release". *Surf Interfaces*, **64**:106445, 2025.

[11] A.B. Soni, G. Satishkumar, and M.W.C. Man. "Palladium Nanoparticles Stabilized in Ionic Liquid-Based Periodic Mesoporous Organosilica: An Efficient Heterogeneous Catalyst for Oxidative Acylation of Ketones". *Chemistry Select*, **9**(44):e202403464, 2024.

[12] B.J. Melde, B.T. Holland, C.F. Blanford, and A. Stein. "Mesoporous sieves with unified hybrid inorganic/organic frameworks". *Chem Mater.*, **11**(11):3302–8, 1999.

[13] T. Asefa, M.J. MacLachlan, N. Coombs, and G.A. Ozin. "Periodic mesoporous organosilicas with organic groups inside the channel walls". *Nature.*, **402**(6764):867–71, 1999.

[14] S.M.H. Moghaddam, M. Haghighat, and F. Shirini. "Ionic liquid-based periodic mesoporous organosilicas: Metal/solvent-free synthesis of formamides and formamidines". *J Mol Struct.*, **1274**:134473, 2023.

[15] B. Karimi, N. Ganji, O. Pourshiani, and W.R. Thiel. "Periodic mesoporous organosilicas (PMOs): From synthesis strategies to applications". *Prog Mater Sci.*, **125**:100896, 2022.

[16] N. Mizoshita, T. Tani, and S. Inagaki. "Syntheses, properties and applications of periodic mesoporous organosilicas prepared from bridged organosilane precursors". *Chem Soc Rev.*, **40**(2):789–800, 2011.

[17] Q. Yang, J. Liu, L. Zhang, and C. Li. "Functionalized periodic mesoporous organosilicas for catalysis". *J Mater Chem.*, **19**(14): 1945–55, 2009.

[18] M. Haghighat, M. Golshekan, and F. Shirini. "Periodic mesoporous organosilica containing bridged N-Sulfonic acid groups: Promotion of the synthesis of N, N′-diarylformamidines, benzoxazoles, benzothiazoles and benzimidazoles". *Chem Select.*, **4**(27):7968–75, 2019.

[19] A.D. Handoko, K.D. Fredrickson, B. Anasori, K.W. Convey, L.R. Johnson, Y. Gogotsi, et al. "Tuning the basal plane functionalization of two-dimensional metal carbides (MXenes) to control hydrogen evolution activity". *ACS Appl Energ Mater.*, **1**(1):173–80, 2017.

[20] S. Xu, X. Zhang, T. Zheng, Z. Zhao, C. Shang, Z. Hu, M. Dong, Y. Qiao, C. Bai, and X. Zhang. "Advancements in high-performance MXene composite fibers integrated with various functional materials: Fabrication, functionalization, property enhancement, and applications". *J Mater Sci Technol.*, **252**(1), 2025.

[21] Z. Cai and H. Kim. "Recent advances in MXene gas sensors: synthesis, composites, and mechanisms". *NPJ 2D Mater Appl.*, **9**(1):66, 2025.

[22] L. Huang, K. Hou, X. Jia, H. Pan, and M. Du. "Preparation of novel silver nanoplates/graphene composite and their application in vanillin electrochemical detection". *Mater Sci Eng C*, **38**:39–45, 2014.

[23] M.A. Khabisi, F. Shirini, K. Shirini, H. Khorsand, M. Marian, and A. Rosenkranz. "Additively manufactured MAX-and MXene-composite scaffolds for bone regeneration-recent advances and future perspectives". *Colloid Surface B.*, **225**:113282, 2023.

[24] H. Riazi, S.K. Nemani, M.C. Grady, B. Anasori, and M. Soroush. "Ti_3C_2 MXene–polymer nanocomposites and their applications". *J Mater Chem A.*, **9**(13):8051–98, 2019.

[25] M. Alhabeb, K. Maleski, B. Anasori, P. Lelyukh, L. Clark, S. Sin, et al. "Guidelines for synthesis and processing of two-dimensional titanium carbide ($Ti_3C_2T_x$ MXene).". *Chem Mater.*, **29**(18):7633–44, 2017.

[26] M. Naguib, V.N. Mochalin, M.W. Barsoum, and Y. Gogotsi. "Two-dimensional materials: 25th anniversary article: MXenes: a new family of two-dimensional materials". *Adv Mater.*, **26**(7):982–982, 2014.

[27] M.W. Barsoum. "MAX phases: properties of machinable ternary carbides and nitrides". John Wiley & Sons, 2013.

[28] M. Alhabeb, K. Maleski, T.S. Mathis, A. Sarycheva, C.B. Hatter, S. Uzun, et al. "Selective etching of silicon from Ti_3SiC_2 (MAX) to obtain 2D titanium carbide (MXene)". Mxenes: Jenny Stanford Publishing:451–62, 2023.

[29] C.E. Shuck, M. Han, K. Maleski, K. Hantanasirisakul, S.J. Kim, J. Choi, et al. "Effect of Ti_3AlC_2 MAX phase on structure and properties of resultant $Ti_3C_2T_x$ MXene". *ACS Appl Nano Mater.*, **2** (6):3368–76, 2019.

[30] N. Singh and J. Pandey. "DABCO catalyzed, green and efficient, one-pot multicomponent synthesis of 5-aminopyrazole-4-carbonitrile". *CRGSC.*, **4**:100134, 2021.

[31] M.U. Rehman, F. He, X. Shu, J. Guo, Z. Liu, S. Cao, and S. Long. "Antibacterial and antifungal pyrazoles based on different construction strategies". *Eur J Med Chem*, **282**:117081, 2025.

[32] S. Hanifi, M.G. Dekamin, and M. Eslami. "Magnetic $BiFeO_3$ nanoparticles: a robust and efficient nanocatalyst for the green one-pot three-component synthesis of highly substituted 3, 4-dihydropyrimidine-2(1*H*)-one/thione derivatives". *Sci Rep.*, **14**(1): 22201, 2024.

[33] G. Li, Y. Cheng, C. Han, C. Song, N. Huang, and Y. Du. "Pyrazole-containing pharmaceuticals: target, pharmacological activity, and their SAR studies". *RSC Med Chem.*, **13**(11):1300–21, 2022.

[34] T.M. Krygowski, R. Anulewicz, M.K. Cyrański, and D. Puchala, A. Rasala. "Separation of the energetic and geometric contribution to the aromaticity. Part IX. Aromaticity of pyrazoles in dependence on the kind of substitution". *Tetrahedron*, **54**(40):12295–300, 1998.

[35] K. Rue and R.G. Raptis. "Low-temperature crystal structure of 4-chloro-1*H*-pyrazole". *Structure Reports*, **77**(9):955–7, 2021.

[36] S. Thore, S.V. Gupta, and K.G. Baheti. "Novel ethyl-5-amino-3-methylthio-1*H*-pyrazole-4-carboxylates: Synthesis and pharmacological activity". *J Saudi Chem Soc.*, **20**(3):259–64, 2016.

[37] M. Liu, J. Li, H. Chai, K. Zhang, D. Yang, Q. Zhang, et al. "A convenient four-component one-pot strategy toward the synthesis of pyrazolo [3,4-d] pyrimidines". *Beilstein J Org Chem.*, **11**(1): 2125–31, 2015.

[38] F. Nemati, S.H. Nikkhah, and A. Elhampour. "An environmental friendly approach for the catalyst-free synthesis of highly substituted pyrazoles promoted by ultrasonic radiation". *Chinese Chem Lett.*, **26** (11):1397–9, 2015.

[39] S. Gupta, L.M. Rodrigues, A.P. Esteves, A.M. Oliveira-Campos, M.S.J. Nascimento, N. Nazareth, et al. "Synthesis of *N*-aryl-5-amino-4-cyanopyrazole derivatives as potent xanthine oxidase inhibitors". *Euro J Med Chem.*, **43**(4):771–80, 2018.

[40] A. Alizadeh and A. Roosta. "A convenient approach for the synthesis of 1, 3-diphenyl-1*H*-pyrazole-5-carbonitrile". *Synlett.*, **27**(17):2455–8, 2016.

[41] H.M. Elnagdy and D. Sarma. "$FeCl_3$/PVP as Green Homogeneous Catalyst to Synthesize 5-Amino-1*H*-Pyrazole-4-Carbonitriles from Malononitrile Derivatives". *Chem Select*, **4**(3):783–7, 2019.

[42] M. Mashhadinezhad, F. Shirini, and M. Mamaghani. "Nanoporous Na^+-montmorillonite perchloric acid as an efficient heterogeneous catalyst for synthesis of merocyanine dyes based on isoxazolone and barbituric acid". *Micropor Mesopor Mat.*, **262**:269–82, 2018.

[43] M. Seddighi, F. Shirini, and M. Mamaghani. "Sulfonated rice husk ash (RHA-SO_3H) as a highly efficient and reusable catalyst for the synthesis of some bis-heterocyclic compounds". *RSC Adv.*, **3**(46): 24046–53, 2013.

[44] M.M. Surchani, F. Shirini, H. Tajik, and O.G. Jolodar. "2, 2â-Bipyridine: An efficient organo-catalyst for the synthesis of pyrano [2, 3-d] pyrimidine and pyrido [2, 3-d] pyrimidine derivatives". *Iranian J Cat.*, **14**(3), 2024.

[45] S. Hideshima, Y. Kawasaki, D. Takimoto, Y. Gogotsi, and W. Sugimoto. "Size-dependent electrochemical properties of vertically aligned MXene electrodes for fast Li-ion storage". *Electrochimica Acta*, **519**:145849, 2025.

[46] P. Arora and J.K. Rajput. "One-pot multicomponent click synthesis of pyrazole derivatives using cyclodextrin-supported capsaicin nanoparticles as catalyst". *J Mater Sci.*, **52**(19):11413–27, 2017.

[47] H. Kiyani and M. Bamdad. "Sodium ascorbate as an expedient catalyst for green synthesis of polysubstituted 5-aminopyrazole-4-carbonitriles and 6-amino-1, 4-dihydropyrano [2, 3-c] pyrazole-5-carbonitriles". *Res Chem Intermediate.*, **44**(4):2761–78, 2018.

[48] A. Sapkal and S. Kamble. "Sodium toluene-4-sulfonate as a reusable and eco-friendly catalyst for greener synthesis of 5-aminopyrazole-4-carbonitrile in aqueous medium". *J Heterocyclic Chem.*, **57**(10): 3597–604, 2020.

[49] M. Soleimani, T. Akbarpour, and A. Khazaei. "Fabrication of Copper (II)-coated Magnetic Core-shell Nanoparticles an Engineered Nano-magnetic Catalyst for the Synthesis of Pyrano Pyrazole and Pyrazole Derivatives". *Polycycl Aromati Comp.*, **44**(1):90–116, 2024.

[50] A. Gorji, T. Akbarpour, and A. Khazaei. "Synthesis of hexahydroquinolines, 5-amino-1, 3-diphenyl-1*H*-pyrazole-4-carbonitrile and 1-aminoalkyl-2-naphthols derivatives using an engineered copper-based nano-magnetic catalyst (Fe_3O_4@ CQD@ Si (OEt)$(CH2)_3$NH@CC@Ad@Cu $(OAc)_2$)". *Polycycl Aromat Comp.*, **43**(6):5041–73, 2023.

[51] N. Singh and J. Pandey. "DABCO catalyzed, green and efficient, one-pot multicomponent synthesis of 5-aminopyrazole-4-carbonitrile". *Current Research in Green and Sustainable Chemistry*, **4**:100134, 2021.

[52] A.R. Obaid and L. Shiri. "Synthesis, Characterization, and Application of $CoFe_2O_4$@ SiO_2@ CPTES@ Melamine Nanoparticles as a Magnetic Catalyst for the Synthesis of Pyrazole Derivatives". *J Appl Organometall Chem.*, **4**:178–89, 2024.

[53] A.R. Moosavi-Zare, M. Rezaei-Gohar, M. Tavasoli, and H. Goudarzi-afshar. "The synthesis of 5-amino-1*H*-pyrazole-4-carbonitriles by anomeric-based oxidative aromatization over [CSPy] $ZnCl_3$ as a new catalyst". *Res on Chem Intermediate*, **47**(7):2689–700, 2021.

Supplementary

Experimental details

Materials and methods

All substrates used in this study, including ethanol, tetraethyl orthosilicate (TEOS- Meck), Pluronic P123 (average Mn $\sim$ 14,600- Merck), bis[3-(trimethoxysilyl) propyl] amine (BTPA- Merck), hydrochloric acid (HCl 37%- Merck), lithium fluoride (LiF- 99.99 Suprapur- Merck), Maxphase (Ti_3CAl_2- purity of $\geq$ 98%, 200 meshes purchased from Ningbo Beijiaer New Material Co., Ltd.), 3-aminopropyl triethoxysilane (99% Merck), and various aldehydes, were purchased from Sigma, Aldrich, and Merck Chemical Companies. Pure distilled water and 96% ethanol were used as solvents.

Characterization

Thin-layer chromatography (TLC) experiments were conducted using a UV lamp emitting at a wavelength of 254 nm. Product identification was performed using a Shimadzu FTIR 8400S spectrometer with potassium bromide (KBr) disks. Additionally, ^{1}HNMR spectra were recorded on a Bruker Avance 500 spectrometer in DMSO-d_6 at ambient temperature. Melting points were determined using a 9100 Electrothermal apparatus, and values are reported without corrections. The yields provided are based on the purified products obtained after the purification process.

The electron impact mass spectrum of the compound $C_{17}H_{14}N_4O_2$ (molecular weight 306 g/mol) displays a well-defined fragmentation pattern that is consistent with the proposed molecular structure. The protonated molecular ion is observed at m/z 312.0 ($[M+H]^+$), confirming the molecular weight. Additional high-mass fragments appear at m/z 287.4 and 265.4, which can be attributed to sequential losses of water ($[M - H_2O]^+$) and the cyano group ($[M - CN]^+$), respectively. These peaks highlight the lability of the hydroxyl substituent and the nitrile moiety under ionization conditions.

The most intense signal in the spectrum, corresponding to the base peak, is detected at m/z 133.1. This fragment represents a highly stable cation formed through cleavage at the triazole core, reflecting the intrinsic stability of heteroaromatic cations generated from this substructure. Complementary aromatic fragments are found in the m/z 149 – 178 range, consistent with oxygenated benzyl species derived from the indole-like aromatic portion of the molecule. The peaks at m/z 83.2, 105.3, and 119.1 are characteristic of smaller aromatic cations originating from the phenyl substituent.

Together, these fragmentation pathways suggest that the compound undergoes stepwise dissociation, initiated by the loss of small substituents (–OH, –CN, –CH_3) and followed by bond cleavage between the triazole nucleus and adjacent aromatic groups. The resulting fragments are stabilized either through resonance delocalization across the aromatic rings or by heteroatom participation in charge distribution. The predominance of the m/z 133.1 ion emphasizes the structural role of the triazole moiety in governing fragmentation stability.

Overall, the spectrum provides strong support for the proposed molecular framework of $C_{17}H_{14}N_4O_2$, with the key diagnostic peaks (m/z 312.0, 287.4, 265.4, 178.2, and 133.1) serving as reliable markers for structural elucidation and confirmation in analytical studies.

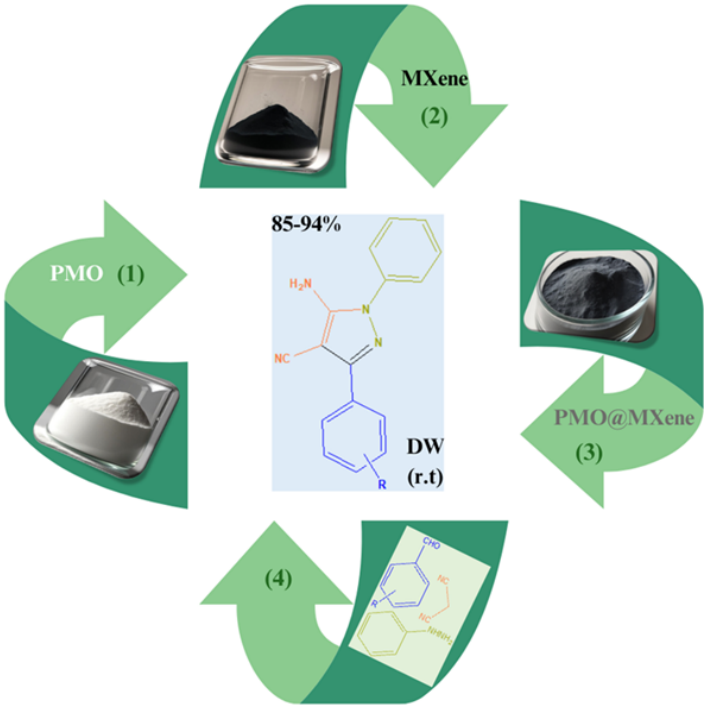

Supplementary Figure 1. General scheme of the PMO@MXene nanocatalyst synthesis and its use in the synthesis of 5-amino-3-(aryl)-1-phenyl-1-*H*-pyrazole-4-carbonitrile (pyrazole) derivatives (Graphical abstract)

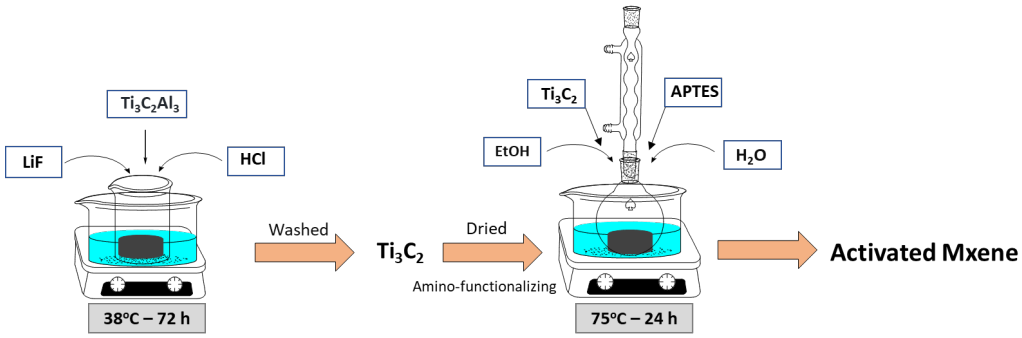

Supplementary Scheme 1. Schematic of the synthesis of the MXene and amino-functionalized MXene.

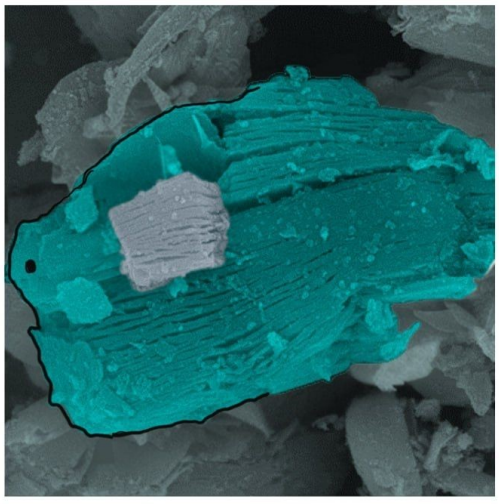

Supplementary Scheme 2. FESEM image of MXene, like a fish, designed by the Nanoart method.

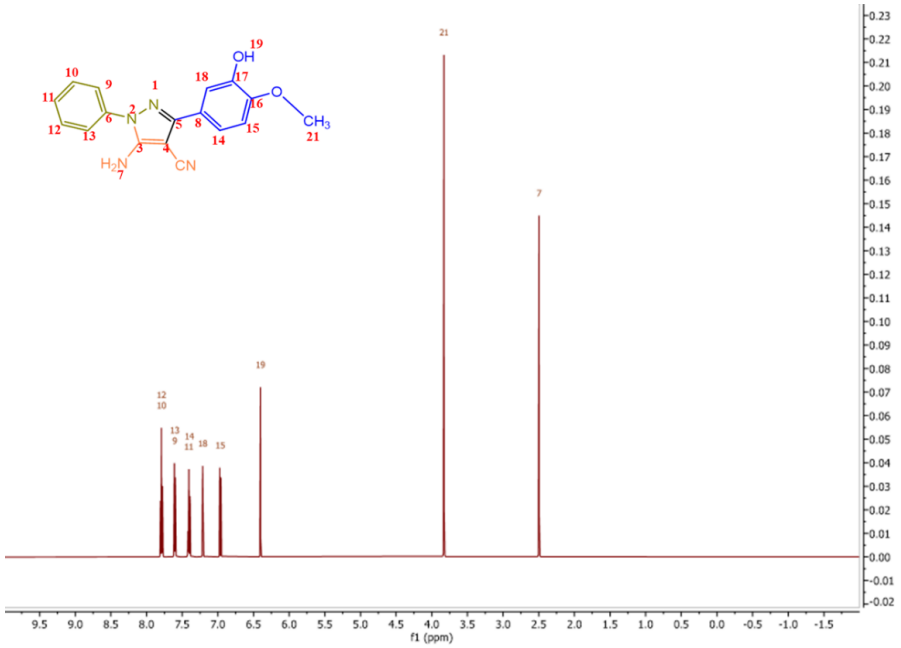

Supplementary Figure 2. H[1]NMR of 5-Amino-(3-hydroxy-4-methoxyphenyl)-1-phenyl-1*H*-pyrazole-4-carbonitrile.

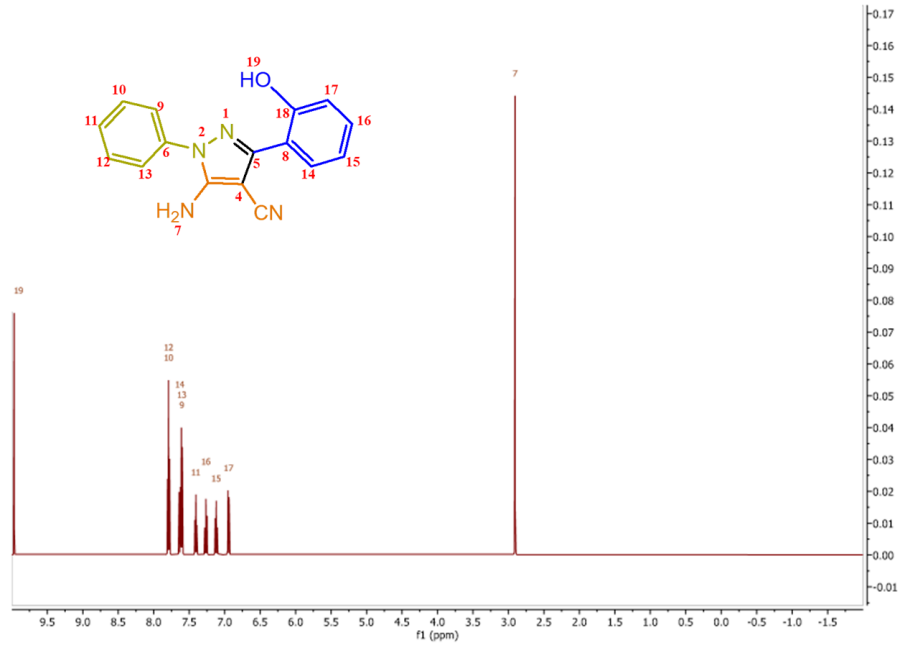

Supplementary Figure 3. H[1]NMR of 5-Amino-3-(2-hydroxyphenyl)-1-phenyl-1*H*-pyrazole-4-carbonitrile.

2008-9244[https://doi.org/10.57647/jnsc.2025.1505.19]

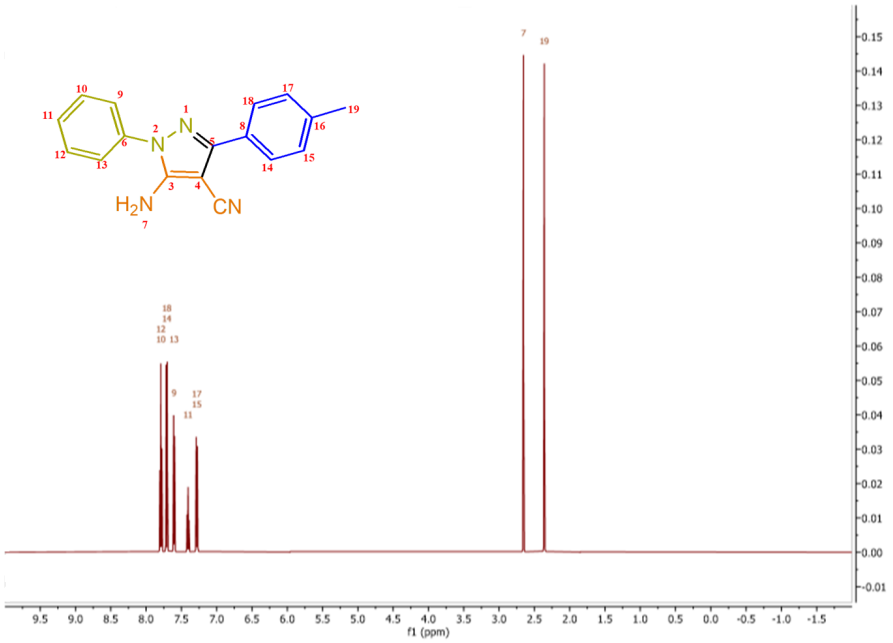

Supplementary Figure 4. H[1]NMR of 5-Amino-1-phenyl-3-(p-tolyl)-1*H*-pyrazole-4-carbonitrile.

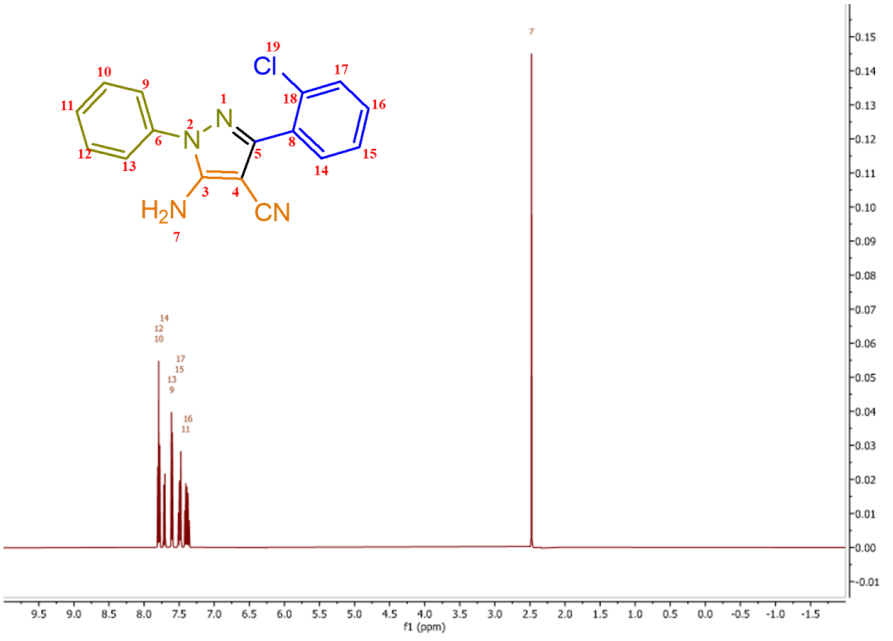

Supplementary Figure 5. H[1]NMR of 5-Amino-3-(2-chlorophenyl)-1-phenyl-1*H*-pyrazole-4-carbonitrile.

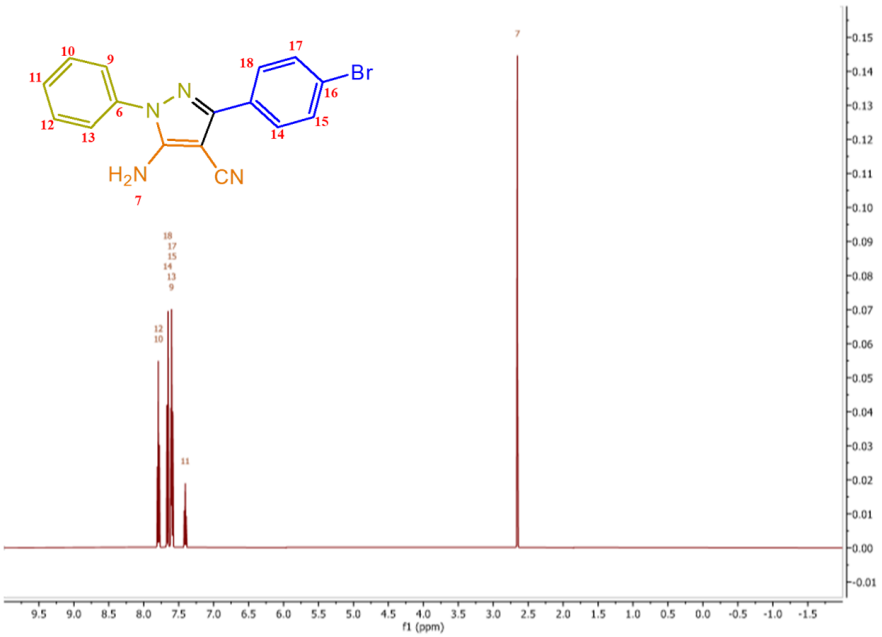

Supplementary Figure 6. H^1NMR of 5-Amino-3-(4-bromophenyl)-1-phenyl-1*H*-pyrazole-4-carbonitrile.

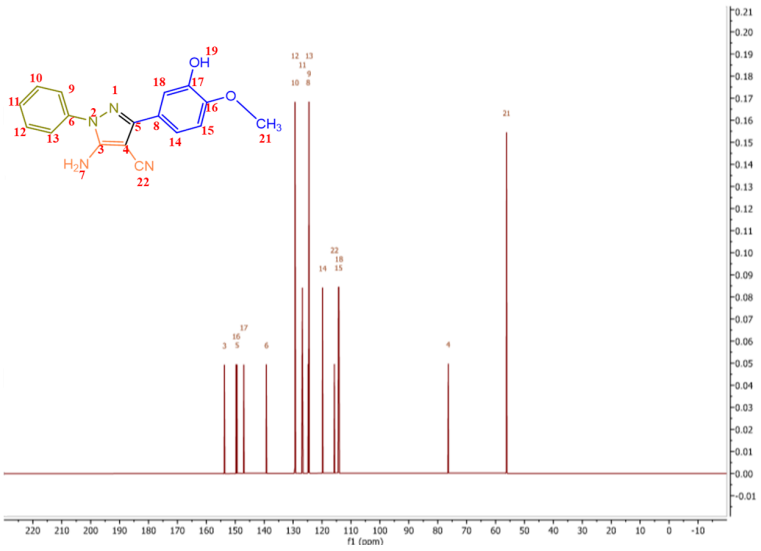

Supplementary Figure 7. ^{13}CNMR of 5-Amino-(3-hydroxy-4-methoxyphenyl)-1-phenyl-1*H*-pyrazole-4-carbonitrile.

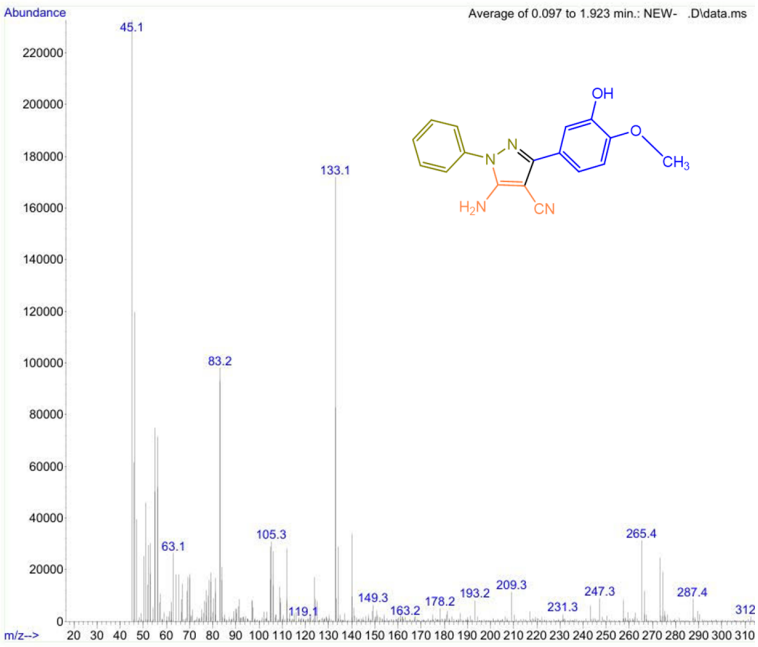

Supplementary Figure 8. MASS spectroscopy of 5-Amino-(3-hydroxy-4-methoxyphenyl)-1-phenyl-1*H*-pyrazole-4-carbonitrile..

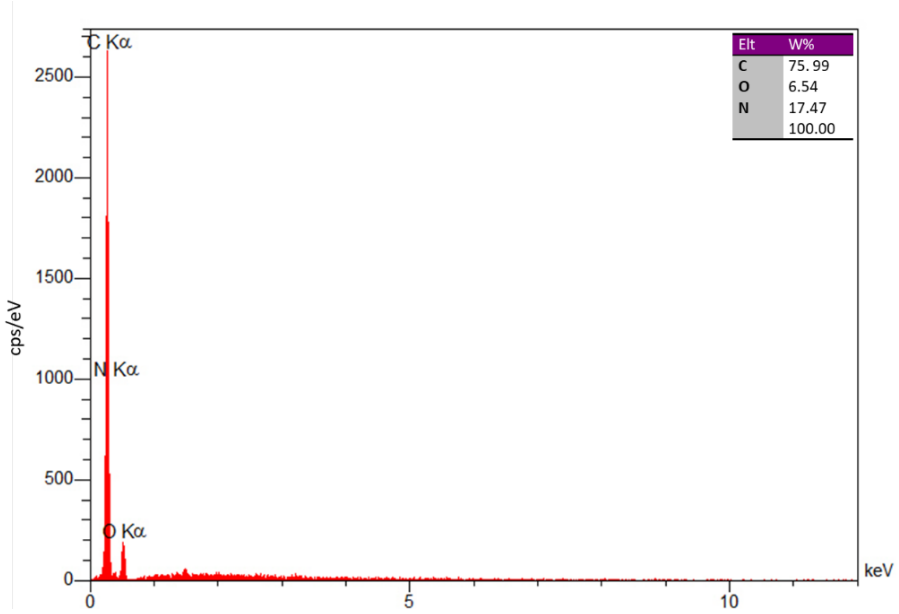

Supplementary Figure 9. Elemental analysis of 5-Amino-(3-hydroxy-4-methoxyphenyl)-1-phenyl-1*H*-pyrazole-4-carbonitrile.